Published online 15 December 2007

Nucleic Acids Research, 2008, Vol. 36, No. 3 ***849–860***
doi:10.1093/nar/gkm1101

Solution structures of 2:1 and 1:1 DNA polymerase–DNA complexes probed by ultracentrifugation and small-angle X-ray scattering

Kuo-Hsiang Tang[1,2], Marc Niebuhr[3], Ann Aulabaugh[4] and Ming-Daw Tsai[1,2,5,*]

[1]Department of Chemistry and Department of Biochemistry, the Ohio State University, Columbus, OH 43210, USA, [2]Genomics Research Center, Academia Sinica, Taiwan, [3]Stanford Synchrotron Radiation Laboratory, MS99, SLAC, Menlo Park, CA 94025, [4]Wyeth Research Biophysics/Enzymology-Screening Sciences, Pearl River, NY 10965, USA and [5]Institute of Biological Chemistry, Academia Sinica, Taiwan

Received November 9, 2007; Revised and Accepted November 25, 2007

ABSTRACT

We report small-angle X-ray scattering (SAXS) and sedimentation velocity (SV) studies on the enzyme–DNA complexes of rat DNA polymerase β (Pol β) and African swine fever virus DNA polymerase X (ASFV Pol X) with one-nucleotide gapped DNA. The results indicated formation of a 2:1 Pol β–DNA complex, whereas only 1:1 Pol X–DNA complex was observed. Three-dimensional structural models for the 2:1 Pol β–DNA and 1:1 Pol X–DNA complexes were generated from the SAXS experimental data to correlate with the functions of the DNA polymerases. The former indicates interactions of the 8 kDa 5′-dRP lyase domain of the second Pol β molecule with the active site of the 1:1 Pol β–DNA complex, while the latter demonstrates how ASFV Pol X binds DNA in the absence of DNA-binding motif(s). As ASFV Pol X has no 5′-dRP lyase domain, it is reasonable not to form a 2:1 complex. Based on the enhanced activities of the 2:1 complex and the observation that the 8 kDa domain is not in an optimal configuration for the 5′-dRP lyase reaction in the crystal structures of the closed ternary enzyme–DNA–dNTP complexes, we propose that the asymmetric 2:1 Pol β–DNA complex enhances the function of Pol β.

INTRODUCTION

Most of the DNA polymerase functional studies and structural studies have focused on the fidelity of nucleotide (dNTP) insertion into the DNA polymerase–DNA complex. Relatively less is known about the conformation of DNA polymerase–DNA complexes and DNA polymerase–DNA interactions in solution. Although most of the known DNA polymerases are characterized as a monomeric form in the presence or absence of DNA in crystallization studies (1,2), the DNA polymerase–DNA complex with the ratio of 2:1 has been detected in solution using Surface Plasmon Resonance biosensor (3), fluorescence titration and analytical ultracentrifugation (4–6). The structure of the 2:1 complex has yet to be characterized, and the relationship between the 2:1 complex in solution reported by these studies and the 1:1 complex revealed by the crystal structures has yet to be addressed. Moreover, there have been very few discussions about whether the reported 2:1 complex is functionally relevant.

In this report, we used small-angle X-ray scattering (SAXS) and sedimentation velocity (SV) to investigate the solution structures of the following two DNA polymerase–DNA complexes: rat (*Rattus norvegicus*) DNA polymerase β (Pol β), and African swine fever virus DNA polymerase X (ASFV Pol X). Pol β is a 39 kDa monomeric DNA polymerase (PDB code 1BPD, Figure 1A) (1) responsible for the base excision repair (BER) pathway in mammalian cells (7). It possesses a 5′-deoxyribose phosphodiesterase (5′-dRP lyase) activity with the 8 kDa lyase domain, and a nucleotidyl transferase activity with the 31 kDa polymerase domain that contains the DNA-binding, nucleotidyl transferase and dNTP-binding subdomains. Pol β uses the helix-hairpin-helix (HhH) motifs in the 8 kDa domain and the DNA-binding subdomain to interact with the DNA backbone as shown in the structure of Pol β–DNA complex (PDB code 1BPX) (7,8) (Figure 1B, where the HhH motifs are shown in yellow in Pol β–DNA complex). The DNA-induced conformational change in the 1:1 Pol β–DNA complex (8) is shown in Figure 1B. ASFV Pol X is only half the size of Pol β (20 kDa) and is missing the 8 kDa lyase domain and the dNTP-binding subdomain. Two forms of the free ASFV Pol X have been identified: the oxidized form (PDB code 1JQR), with a disulfide bond

*To whom correspondence should be addressed. Tel: +886 2 2789 9930; Fax: +886 2 2789 8811; Email: tsai@chemistry.ohio-state.edu

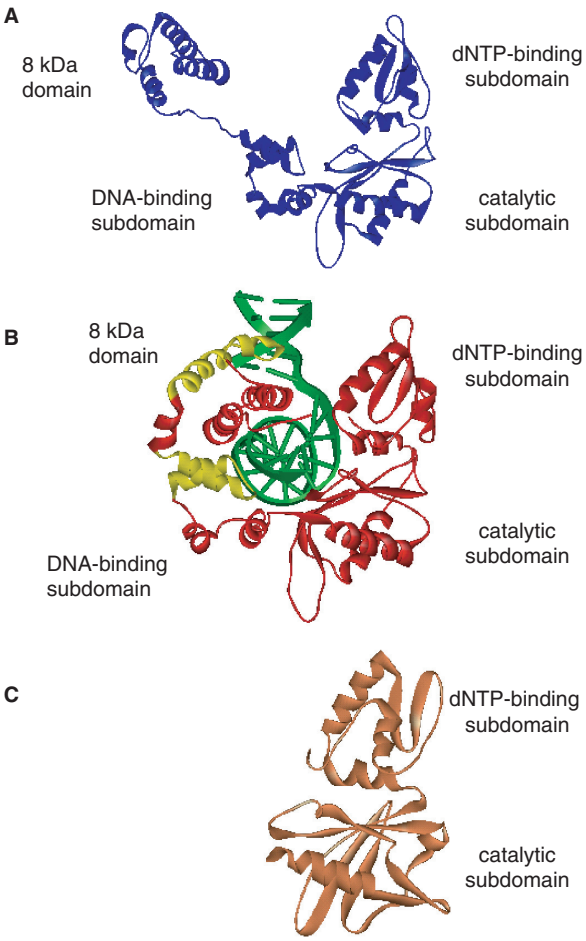

Figure 1. The atomic resolution structures of Pol β and ASFV Pol X. (**A**) The crystal structure of free Pol β (1BPD); (**B**) the Pol β–DNA complex (1BPX). Protein and DNA moieties are shown in red and green, respectively, and the helix-hairpin-helix motifs are shown in yellow and (**C**) the NMR structure of free ASFV Pol X (1JAJ). The 8 kDa lyase domain, DNA-binding, catalytic and dNTP-binding subdomains are labeled. The 8 kDa lyase domain and DNA-binding subdomain in Pol β are absent in ASFV Pol X.

in the catalytic subdomain (9), and the reduced form (PDB code 1JAJ) (Figure 1C), with no disulfide linkage (10). The global structures of these two forms are similar (11,12). ASFV Pol X has been shown to bind DNA as tightly as Pol β, even though it does not contain DNA-binding domains/motifs.

Our studies employed the biologically relevant gapped DNA, which was also used previously in functional and structural studies of Pol β and ASFV Pol X (8,9,13,14). Both SAXS and SV were used to characterize the association state of the complexes, and SAXS used to gain structural information of the DNA polymerase–DNA complex. Coexistence of the 1:1 and 2:1 Pol β–DNA complexes with substoichiometric amounts of DNA (at the ratio of Pol β/DNA from 20/1 to 1/1) was observed, while only the monomeric ASFV Pol X–DNA complex was identified at various ratios of ASFV Pol X/DNA. Different modeling approaches were then used to produce structural models for the previously uncharacterized 2:1 Pol β–DNA and 1:1 ASFV Pol X–DNA complexes. The modeled structures were evaluated by various criteria including functional relevance. These new structural models provide important insight into the enzyme–DNA interactions utilized by the two different classes of polymerases, Pol β and ASFV Pol X. There is also abundant evidence suggesting that the 2:1 Pol β–DNA complex represents the functional form in base excision repair.

MATERIALS AND METHODS

Materials

Pol β and ASFV Pol X samples were over-expressed in *Escherichia coli* and purified as previously described (13,15) with minor modifications. The protein concentration was determined using the extinction coefficient $\varepsilon_{280} = 2.12 \times 10^4\,cm^{-1}\,M^{-1}$ (Pol β) or $1.54 \times 10^4\,cm^{-1}\,M^{-1}$ (ASFV Pol X) and by the Bradford assay. dNTPs were from Amersham Biosciences. DNA oligonucleotides were from IDT (Coralville, IA, USA). The DNA substrate used in this report is 16-mer template/10-mer primer/5-mer downstream primer 1 nt gapped DNA (16/10/5-mer) with the following sequence: template, 5′-CCGACGGCGCATCAGC-3′; primer, 5′-GCTGATG CGC_{dd}-3′; and downstream primer, 5′-pGTCGG-3′. The DNA sequence was identical to that used for crystallographic studies of Pol β (8). G represents the template base pairing the incoming nucleotide, 3′-dd stands for the DNA primer with dideoxynucleotide terminated, which prevents the proceeding of the chemical step. 5′-p stands for 5′-phosphorylated.

Sample preparations

For the DNA titration to Pol β by SAXS, 100 μM Pol β was mixed with increasing concentrations of DNA (0–200 μM), 10 mM DTT, 0.10 M KCl, 10% glycerol and 50 mM MOPS buffer at pH 7.0 at 20°C. The buffer conditions were similar for SV studies of Pol β, except 1 mM DTT and trace amount (<0.1%) glycerol were used. The NMR samples for DNA titration to Pol β were prepared in 0.6 mM ^{15}N-labeled Pol β with increasing concentrations of DNA (0–1.2 mM) in 50 mM phosphate buffer, 0.1 M KCl at pH 7.0. For the DNA titration to ASFV Pol X by SAXS, 50 μM ASFV Pol X was mixed with increasing concentrations of DNA (0–50 μM), 10 mM DTT, 0.50 M KCl, 10% glycerol, and 50 mM MOPS buffer at pH 7.0 at 20°C. 10 mM DTT was included in the ASFV Pol X samples to ensure the enzyme in the reduced form. DTNB (Ellman's reagent) was used to examine if disulfide bond was formed in our samples.

Small-angle X-ray scattering (SAXS)

SAXS experiments were conducted at BL 4-2 of the Stanford Synchrotron Radiation Laboratory (SSRL) (16) and at BioCAT 18-ID of the Advanced Photon Sources (APS) (17). The SAXS measurements were similar to procedures reported previously with minor adjustments (18).

SAXS data analyses and modeling

The Pol β and ASFV Pol X concentration series studies were performed to examine the intermolecular and non-specific (aggregation) interactions (Figure S1). The final scattering curve was obtained by merging the small angle data (Q-range from 0.02 to 0.15 $Å^{-1}$) of the low concentration sample (1–2 mg/ml) with the data in the high angle region (Q-range from 0.10 to 0.73 $Å^{-1}$) of the high concentration data (16 mg/ml) with PRIMUS (19), to minimize inter-particle interaction effects in the low angle region (Figure S1). The forward scattering intensity ($I(0)$) (20), the radius of gyration (R_g), the longest distance within the particle (D_{max}), and the particle distance distribution function ($P(r)$) were obtained from the experimental SAXS data using the program GNOM (21) and the Guinier approximation (22) with $Q_{max} \times R_g \leq 1.3$. While a polydisperse system was assumed in the DNA titration studies, other reported SAXS data were treated as monodisperse systems unless otherwise mentioned. After processing the scattering data with GNOM, the modeling programs DAMMIN (23) (data in the Q-range from 0.02 to 0.35 $Å^{-1}$) and GASBOR (24) (data in the Q-range from 0.02 to 0.73 $Å^{-1}$) were used to determine the overall conformations of the DNA polymerase–DNA complex and free DNA polymerase, respectively.

In the studies of the 2 : 1 Pol β–DNA complex, a series of samples with nominal Pol β/DNA ratio of 1 : 1.8, 1 : 1.9, 1 : 2.0, 1 : 2.1 and 1 : 2.2 were prepared and their R_g values were determined. The sample with the largest R_g was assumed to contain the highest fraction of the 2 : 1 complexes, and the data set was used as the basis for quaternary structure modeling of the 2 : 1 Pol β–DNA complex with the programs DAMMIN and SASREF. In the absence of a reported high resolution structure, the global rigid-body modeling program SASREF (25) was used to model the 2 : 1 Pol β–DNA complex and the ASFV Pol X–DNA complex using experimental SAXS data and atomic coordinate models. No further constraints on the orientation of the subunits towards each other were made. The atomic resolution models of the 1 : 1 Pol β–DNA complex (1BPX) (8) and full-length Pol β (1BPD) or two isolated domains (the 8 kDa N-terminal domain (1DK3) (26) and the 31 kDa C-terminal (1ZQW) domain (27)) were used to generate the 2 : 1 Pol β–DNA complex, and the free ASFV Pol X (1JAJ) (10) and the 16/10/5-mer DNA in 1BPX were used to construct the ASFV Pol X–DNA complex. The program SUPCOMB (28) was used to superimpose either the DAMMIN and SASREF models, or the reconstructed model and the atomic resolution structure. CRYSOL (29) was used to evaluate the scattering pattern of the crystal structures and verify the fit to the SAXS measurements.

Sedimentation velocity (SV)

SV studies were performed on a Beckman XLI/XLA analytical ultracentrifuge. To investigate the effect of DNA on Pol β, DNA was added to Pol β (3.7 μM) at increasing DNA concentrations from 0 to 7.5 or 15 μM. The reverse titration of 1 μM DNA with increasing concentrations of Pol β (0–27 μM) was also performed. The mixtures (400 μl) were loaded into two-channel (1.2 cm path length) carbon-Epon centerpieces in an An-50 Ti or An-60 Ti rotor. Scans were recorded at 20°C with a rotor speed of 35 000 r.p.m. (An-50 Ti rotor) and 40 000 r.p.m. (An-60 Ti rotor). The signal was detected at 260 and 280 nm, characteristic wavelengths for the protein and DNA, respectively, with a spacing of 0.006 cm in the continuous mode. The sedimentation profiles were analyzed to obtain the sedimentation coefficient distributions with the program Sedfit 9.2 (30) and the ratio of Pol β/DNA in the Pol β–DNA complex with the program SEDPHAT (31). The program HYDROPRO (32) was applied to calculate the hydrodynamic parameters using the Pol β crystal structure coordinates to correlate with the parameters obtained from the centrifugation experiments.

RESULTS

Free ASFV Pol X and Pol β are both monomeric in solution

Figure 2A shows that an *ab initio* model of free ASFV Pol X derived from the SAXS data is very similar to the reported NMR structure (10). The predicted SAXS curve and experimental SAXS data of free ASFV Pol X are superimposable (Figure S3A). No concentration-dependent association is detected for free ASFV Pol X (Figure S1A and B). Changes in the very low Q range (0.02–0.035 $Å^{-1}$) as a function of concentration are observed for Pol β (Figure S1C and D). As described in Materials and Methods section, the scattering curves for generating the structural models were obtained by merging the low concentration pattern for the lowest angles with the high concentration pattern for the higher angles, and no negative effects resulting from either attractive interactions or concentration-dependent association were detected. The volume of the reconstructed model of free Pol β obtained with our SAXS data is in excellent agreement with the crystal structure (Figure S1E) and consistent with the monomeric species observed by SV (Figure S1F and G).

ASFV Pol X–DNA aggregates but forms 1 : 1 complex in solution

The NMR cross-peaks are significantly broadened for the 1 : 1 ASFV Pol X–DNA binary complex (Figure S2A) (9). As a consequence, the solution structure of 1 : 1 ASFV Pol X–DNA binary complex cannot be readily solved by NMR with current experimental conditions. However broadening of NMR peaks is only a very qualitative evidence for aggregation, and SAXS can differentiate complex formation from aggregation. With SAXS, concentration-dependent aggregation was clearly shown with 100 μM or greater ASFV Pol X in DNA titration studies, and protein precipitates were observed when ASFV Pol X mixes with DNA under lower ionic strength (~0.1 M KCl). However, use of lower concentration ASFV Pol X (50 μM or less) in high ionic strength buffer (~0.4 M KCl) in the DNA titration to ASFV Pol X studies (Figure S3B) resulted in no aggregation observed by the Guinier fit (22) to the SAXS data (Figure S3C). The increase of $I(0)$ upon

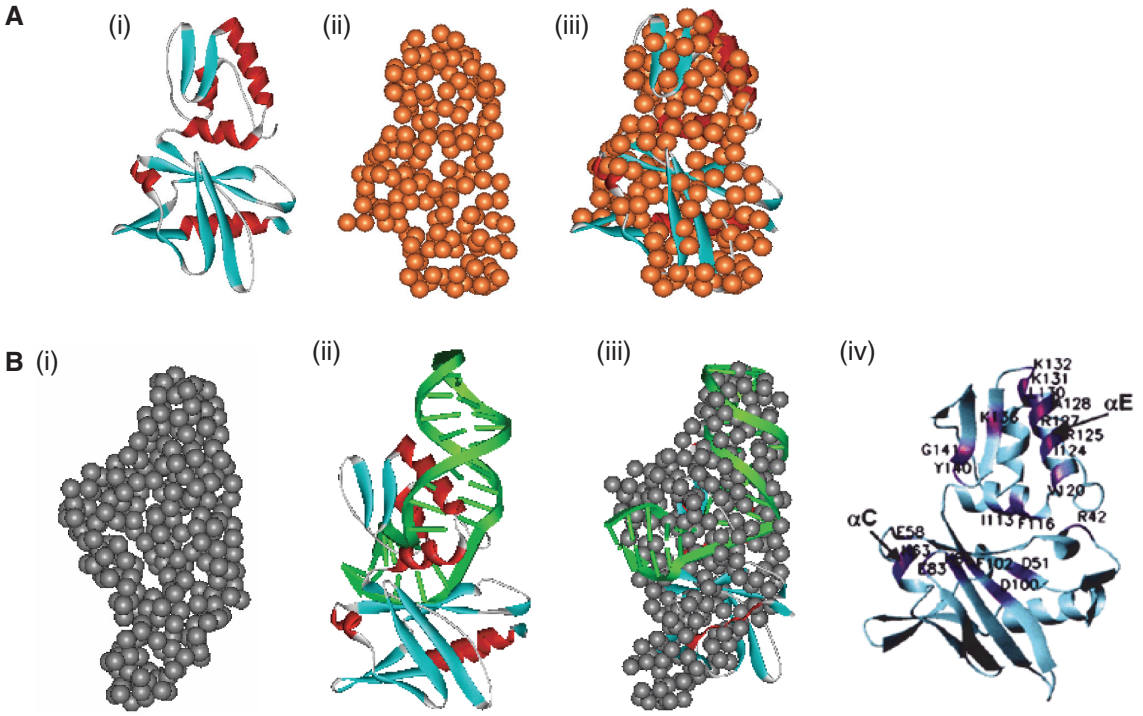

Figure 2. Structural studies of ASFV Pol X and ASFV Pol X–DNA complex. (**A**) (i) The NMR structure of the free ASFV Pol X (1JAJ), (ii) the GASBOR model derived from the SAXS data and (iii) superimpositions of the NMR structure and the GASBOR model. (**B**) The reconstructed model of the ASFV Pol X–DNA complex: (i) the DAMMIN model, (ii) the SASREF model, (iii) overlaid the DAMMIN and SASREF models and (iv) the predicted DNA-binding pocket (the residues involved are labeled) (9).

Table 1. Summary of parameters of Pol β, ASFV Pol X and their binary complexes

Samples[a]	$R_g^{(exptl.)}$ (Guinier)	$R_g^{(exptl.)}$ (GNOM)	$R_g^{(calc.)}$ (CRYSOL)	$D_{max}^{(exptl.)}$ (GNOM)
Pol β studies				
Free E	28.9 ± 0.2	29.1 ± 0.1	28.9 (1BPD)	105 ± 5
1:1 complex	24.0 ± 0.2	23.8 ± 0.2	23.4 (1BPX)	70 ± 5
2:1 complex	36.0 ± 0.3	35.6 ± 0.4	35.0 ± 0.4[b]	135 ± 6
ASFV Pol X studies				
Free E	18.2 ± 0.3	17.8 ± 0.3	17.5 (1JAJ)	60 ± 2
E–DNA complex	21.8 ± 0.3	21.5 ± 0.2	N/A[c]	80 ± 5

The values of R_g and D_{max} are reported in Å.
[a]The 16/10/5-mer 1 nt gapped DNA was used.
[b]Calculated from the reconstructed model shown in Figure 5D.
[c]The computed parameters are not available (N/A) due to lack of the corresponding high-resolution structures.

increasing (DNA) is consistent with formation of the 1 : 1 ASFV Pol X–DNA complex.

The reconstructed model of the 1 : 1 ASFV Pol X–DNA complex

The extended tail in the pair distance distribution function [*P*(r)] plot (Figure S3C), larger ratio of D_{max}/R_g (~3.6, the R_g and D_{max} values, unit in Å are reported in Table 1), and the reconstructed DAMMIN model (Figure 2B) of the ASFV Pol X–DNA complex indicate that the ASFV Pol X–DNA complex is more elongated than the free form, likely from the extended DNA moiety in the complex. The representative SASREF model of the ASFV Pol X–DNA complex is shown in Figure 2B and other models in Figure S3D. The models can be reproducibly reconstructed. The predicted scattering pattern of the SASREF model fits the experimental SAXS data very well (data not shown).

As shown in Figure 2B, the SASREF model is compatible with the DAMMIN model, supporting our hypothesis that the extended tail of the *P*(r) plot and the elongated shape of the DAMMIN model result from the DNA moiety of the ASFV Pol X–DNA complex. Moreover, the SASREF model is consistent with the chemical shift perturbations in the 2D-[^{1}H,^{15}N]-HSQC NMR spectra of the ASFV Pol X–DNA complex reported previously [Figure 2B-(iv)] (9). In the absence of the 8 kDa lyase domain and DNA-binding subdomain, our model indicates that DNA binds to the interface of the catalytic and dNTP-binding subdomains that comprise the active

site of ASFV Pol X, which is more electropositive compared to the counterpart of Pol β. Based on this model, the following residues, R125, R127, K131, K132 and K136, most likely interact with DNA. In contrast, Pol β–DNA interactions depend on the hydrogen bond interactions through the HhH motifs on the 8 kDa lyase domain and DNA-binding subdomain (33).

Pol β–DNA does not aggregate but forms 2 : 1 and 1 : 1 complexes in solution

In contrast to ASFV Pol X–DNA (Figure S2A), the 2D-[^{1}H,^{15}N]-TROSY-HSQC NMR of the 1 : 1 Pol β–DNA complex did not show line broadening (Figure S2B), suggesting lack of aggregation. However, line broadening and signal loss was observed when Pol β is in excess of DNA (Figure S2C), which was attributed to formation of 2 : 1 Pol β–DNA complex (as well as possible exchange between different species) by SAXS analyses, as explained below.

Figure S4A shows the SAXS experimental data of Pol β in the presence of different ratios of DNA. Figure S4B shows that the SAXS experimental data of 100 μM Pol β and 0, 100, 150 and 200 μM DNA are in good agreement with the SAXS curves predicted from a mixture of three components—the free Pol β (1BPD), 1 : 1 Pol β–DNA complex (1BPX) and experimental SAXS data of free DNA. In contrast, the measurements with DNA concentration between 5 and 50 μM cannot be explained with the three-component model, since a clear deviation exists between experimental data and fits in Figure S4C.

If there were only formation of the 1 : 1 Pol β–DNA binary complex, one would expect the large R_g of the elongated free Pol β to slowly decrease upon addition of DNA due to formation of a more compact Pol β–DNA complex. However, the value of R_g actually increases with increasing DNA concentration in the first half of the DNA titration to a Pol β:DNA ratio of 1 : 0.5 (Table S1). The excess scattering in the low Q range could be explained with (i) DNA-induced nonspecific interaction of Pol β or (ii) formation of a larger Pol β–DNA complex with a stoichiometry of 2 : 1 or greater. The first interpretation cannot explain the decrease in R_g when the Pol β:DNA ratio increases from 1 : 0.5 to 1 : 1. The experiments were repeated using a lower concentration of sample and very similar results were obtained (data not shown), indicating that the larger particle was not an aggregate. Thus the second interpretation is more likely.

SAXS analyses of the titration data suggest that the larger Pol β–DNA complex is the 2 : 1 complex. The experimental $I(0)$ fit better with the calculated $I(0)$ from a four-component model (free Pol β, free DNA, the 1 : 1 and 2 : 1 complexes) than a three-component model (described above) (Figure 3, where the experimental and calculated data are connected in bold and dash lines, respectively). Since $I(0)$ is determined by the molecular mass, a larger $I(0)$ value is expected for the 2 : 1 complex compared to the 1 : 1 complex and free Pol β. Aggregation is not indicated for the 2 : 1 complex by Guinier analyses (22), and the experimental data fit is significantly improved when the 2 : 1 complex scattering is taken into consideration (Figure S4D).

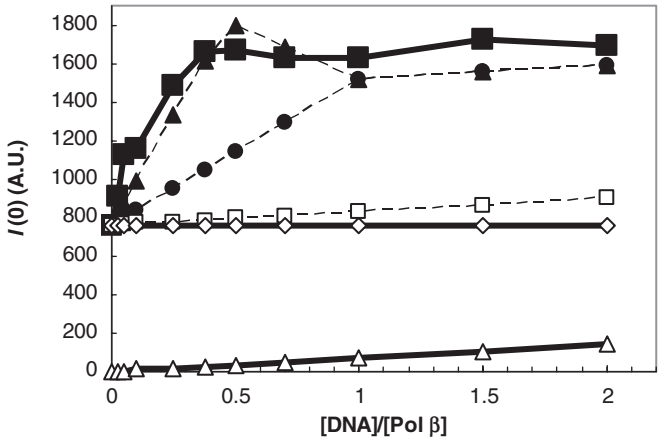

Figure 3. Comparisons of the experimental and calculated $I(0)$ values from the DNA titration to Pol β. The calculated $I(0)$ for the three-components model (free Pol β, free DNA and the 1 : 1 complex) (filled circle), the four-components model (free Pol β, free DNA, the 1 : 1 and 2 : 1 complexes) (filled triangle), no complex formation (open square), and the experimental $I(0)$ for free Pol β(open diamond), free DNA (open triangle), and DNA titration to Pol β(filled square) are shown. The experimental and calculated data points are connected with bold and dash lines, respectively.

Table 2. Sedimentation velocity for Pol β–DNA interactions

The ratio of Pol β–DNA[a]	Mg present	S Pol β	S DNA	S peak 1	S peak 2	f/f_0[b]
1 : 0	−	2.74				1.43
1 : 0	+	2.74				1.46
1 : 0.05	−	2.74			5.1	1.46
1 : 0.05	+	2.74			5.10	1.55
1 : 0.1	−	2.82			5.1	1.52
1 : 0.1	+	2.82			4.8	1.48
1 : 0.5	−			4.0	4.8	1.76
1 : 0.5	+	2.83			4.3	1.82
1 : 1	−			4.0		1.64
1 : 1	+	2.92			4.2	1.58
1 : 2	−		1.8	4.0		1.64
1 : 2	+		1.9	4.0		1.55
0 : 1	−		1.8			1.59
0 : 1	+		1.9			1.57

[a]Pol β of 3.8 μM was used in the experiments.
[b]f: measured frictional coefficient of Pol β; f_0: frictional coefficient for an unhydrated spherical molecule of the same mass.

Further insight of Pol β-DNA interactions from sedimentation velocity

SV experiments were performed to gain additional insight into the number of species present in solution and the hydrodynamic properties of the Pol β–DNA complexes. SEDPHAT (31) was used to determine the stoichiometry of the Pol β–DNA complex using multiple signal detection sedimentation velocity experiments. In the DNA titration to Pol β (Table 2), free Pol β migrated with a sedimentation coefficient of 2.7 S. Upon addition of substoichiometric concentrations of gapped DNA, a new species was observed with a sedimentation coefficient of

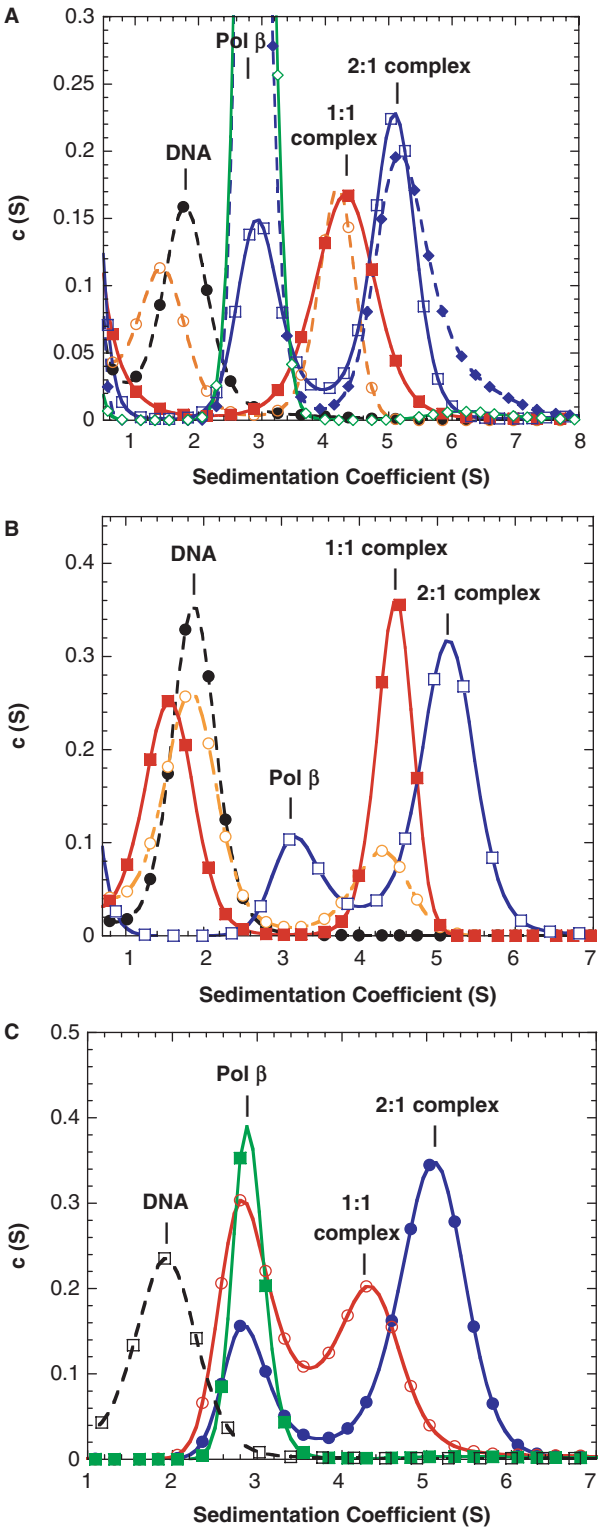

Figure 4. Sedimentation coefficient distribution plots for Pol β titration to DNA. (**A**) The experiments, monitored at 280 nm, were conducted at 1 μM DNA with 0 (filled circle, dashed lines), 1 (open circle, dashed lines), 3 (filled square, continuous lines), 9 (open square, dashed lines) and 27 (filled diamond, dashed lines) μM of Pol β. The c(S) data of 27 μM Pol β is shown in (open diamond, continuous lines). (**B**) The experiments, monitored at 260 nm, were conducted at 1 μM DNA with 0 (filled circle, dashed lines), 0.4 (open circle, dashed lines), 0.8 (filled square, continuous lines) and 7.2 (open square, continuous lines) μM Pol β. (**C**) The ionic strength effect studies were performed with the following samples: 1 μM DNA/9 μM Pol β with 0.1 (filled circle, continuous lines) and 0.4 M (open circle, continuous lines) KCl. The c(S) data of 9 μM Pol β in 0.1 M KCl (filled square, continuous lines) and 1 μM DNA in 0.4 M KCl (open square, dashed lines) are also plotted.

5.1 S with a molecular mass of ~76 kDa, consistent with a 2 : 1 complex. As more DNA was added, new peaks were observed with sedimentation coefficient values intermediate between 5.2 S (the 2 : 1 complex) and 2.7 S (free Pol β). In the presence of stoichiometric and excess DNA, the complex migrated with a sedimentation coefficient of 4.0 S with a molecular mass of ~45 kDa (the 1 : 1 complex). The frictional ratio of the 1 : 1 and 2 : 1 complex has been estimated, and the value for the 2 : 1 complex reflects an elongated shape, consistent with the structural models constructed from SAXS studies (described below).

We next investigated the Mg^{2+} effect on the formation of the Pol β–DNA complexes. In the presence of 10 mM Mg^{2+} (Table 2), the same 5.1 S species was observed at very low DNA levels (Pol β/DNA = 20/1), but as the concentration of DNA increased, there was a continuous shift to lower sedimentation coefficients with increasing DNA until the 4.0 S species was observed at excess DNA to Pol β (Pol β/DNA = 1/2). The results indicate that the 1 : 1 and 2 : 1 complexes are in a faster exchange process (weaker binding) with 10 mM Mg^{2+}, in contrast to a slow exchange process in the absence of Mg^{2+}.

With the reverse titration of Pol β to DNA, similar species are observed and the results are in good agreement with the DNA titration to Pol β (Figure 4 and Table 2). When the ratio of DNA/Pol β is close to 1, the main component was the 4.1 S species (the 1 : 1 complex). As the ratio of Pol β/DNA increases, the species observed in solution correspond to free Pol β and the 5.2 S species (the 2 : 1 complex). As Pol β/DNA reaches 27/1, the only two species observed were the 2.9 S (free Pol β) and the 5.2 S species, implying that no more than two Pol β molecules bind to DNA (Figure 4A and B). This result is consistent with two classes of Pol β-binding sites. As the SV data are influenced by the size and shape of the various sedimenting species, two wavelengths detection, 280 nm (Figure 4A) and 260 nm (Figure 4B), was used to deconvolute the stoichiometry of the Pol β–DNA complex by analysis of the data with SEDPHAT.

Increasing ionic strength shifted the 5.2 S species to the 4.0 S species at 0.4 M KCl (Figure 4C). This result is consistent with the Mg^{2+} effect described above. As high ionic strength buffer is frequently used in crystallographic studies, our results provide a rationale for lack of the crystal structure of the 2 : 1 complex of Pol β and other DNA polymerases. In addition, as the Pol β–DNA–dNTP ternary complex is the functional form, we investigated the hydrodynamics of the 2 : 1 Pol β–DNA complex (when [Pol β]/[DNA] was 6/1) upon addition of dNTP. Addition of 150 μM dCTP (the correct incoming dNTP) and 10 mM Mg^{2+} to the 2 : 1 Pol β–DNA complex did not have a significant effect on the c(S) distribution relative to the sample minus dCTP, suggesting no significant changes in the compositions of the ternary complex, but

hydrodynamic changes can be detected in the 2 : 1 complex species, possibly reflecting the dNTP-induced conformational change of the 2 : 1 complex (data not shown). As the binding affinity for a correct dNTP is in the range of 1–10 μM (34,35), 150 μM dCTP is expected to fully saturate the Pol β–DNA complex. In summary, our results have established that under physiological salt and nucleotide concentrations (10 mM Mg^{2+}, 0.10 M KCl, and 150 μM dNTP), the 2 : 1 Pol β–DNA complex is the predominant species if the enzyme is in excess of DNA.

Two reconstructed models of the 2 : 1 Pol β–DNA complex

From the experimental SAXS data, the $P(r)$ plots were generated for free Pol β, free DNA, the 1 : 1 and 2 : 1 complexes to predict the gross features of the molecular shape (i.e. globular, elongated, etc.) (Figure 5A). The plots indicate that free Pol β, free DNA and the 2 : 1 complex are elongated, and that the 1 : 1 complex is more compact. We then generated a low-resolution structure based on the experimental SAXS data using the program DAMMIN (Figure 5B). The elongated shape of the DAMMIN model is also consistent with the larger ratio of D_{max}/R_g for the 2 : 1 complex (~3.7) compared to the 1 : 1 complex (~2.9).

To improve the resolution of the reconstructed model of the 2 : 1 complex, the crystal structures of the free Pol β (1BPD) and the 1 : 1 Pol β–DNA complex (1BPX) were used to build the reconstructed model with SASREF (31). Because the 8 kDa lyase domain is highly flexible, we also built the model using the atomic resolution structures of the 8 kDa N-terminal lyase (26) and 31 kDa C-terminal polymerase domains (27) to replace the structure of the full-length Pol β in the rigid-body modeling. In either approach, the configurations of the 1 : 1 Pol β–DNA complex, the 8 kDa lyase domain, the 31 kDa polymerase domain, and full-length free Pol β were fixed as in the high-resolution structures, and no symmetrical constraints were applied to build the high-resolution model. As a result, two different models were generated by SASREF. In model A (Figure 5C), generated by the full-length Pol β and 1 : 1 complex as a 'two-body' modeling approach, the dNTP-binding and catalytic subdomains of the second Pol β molecule bind to the template-upstream primer duplex DNA. In model B (Figure 5D), generated by the 8 kDa lyase and 31 kDa polymerase domains and the 1 : 1 complex as a 'three-body' approach, the 8 kDa domain of the second Pol β molecule binds to the template-downstream primer duplex DNA and the dNTP-binding subdomain of the 1 : 1 complex. Notably, SASREF can rarely generate the model B-like structural models with the 'two-body' approach (described below).

Model B is the preferred model based on structure and function

As suggested by Petoukhov and Svergun (25), two criteria need to be satisfied to ensure the fidelity of the SASREF models: stability (multiple runs lead to similar results) and functional relevance. In our studies, the calculated SAXS patterns from both models can fit the experimental data well, and the following analyses were applied to differentiate these models.

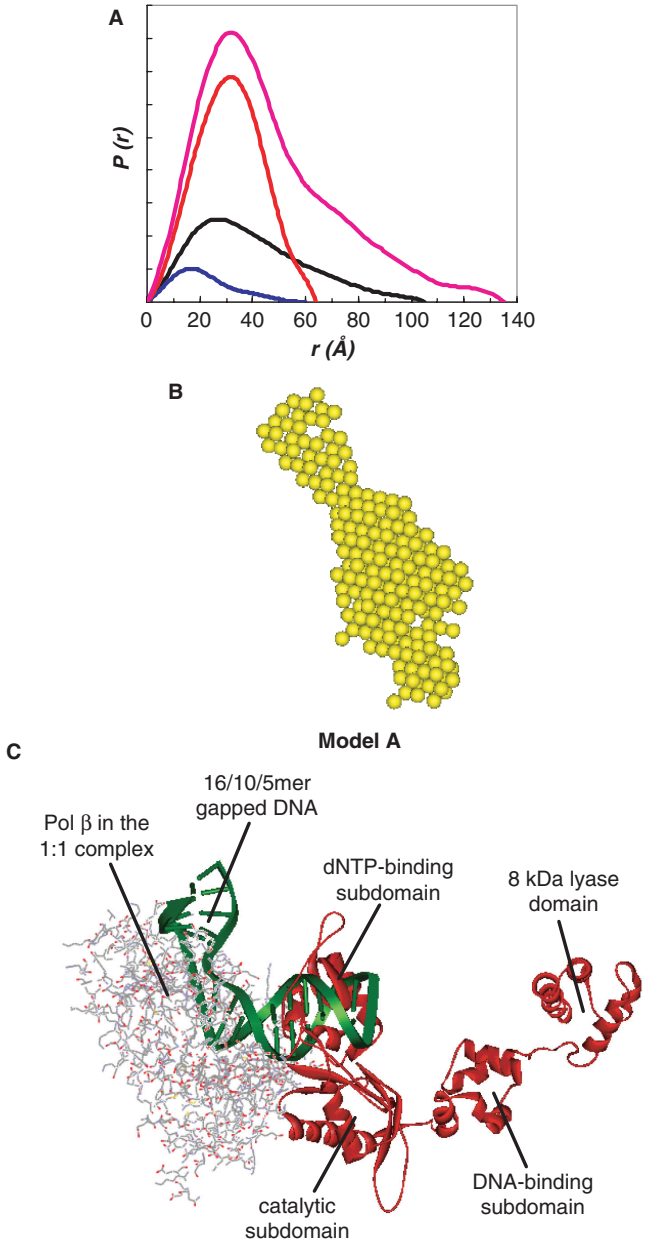

Figure 5. The reconstructed model of the 2:1 complex by SAXS. (**A**) The $P(r)$ plots for free DNA (blue), free Pol β (black), the 1:1 complex (red) and 2:1 complex (magenta). (**B**) The DAMMIN model. (**C**) The SASREF model (model A) built with the 'two-body' approach (see text). (**D**) The SASREF model (model B) built with the 'three-body' approach (see text). The HhH motifs in the 1:1 complex and the second Pol β molecule are shown in pink and yellow, respectively. (**E**) (i) The DAMMIN model, (ii) the SASREF model (model B), (iii) and (iv) superimpositions of the DAMMIN and SASREF models are shown in two orthogonal views.

Stability. More than fifteen SASREF runs were performed for both the 'two-body' model A and the 'three-body' model B approaches. Compared to the 'three-body' approach (examples of the reconstructed models shown in Figure S5B), rather dissimilar 2 : 1 complex structural models were generated by the 'two-body' approach (representative examples shown in Figure S5A). Thus, SASREF model B is evidently more stable than SASREF model A.

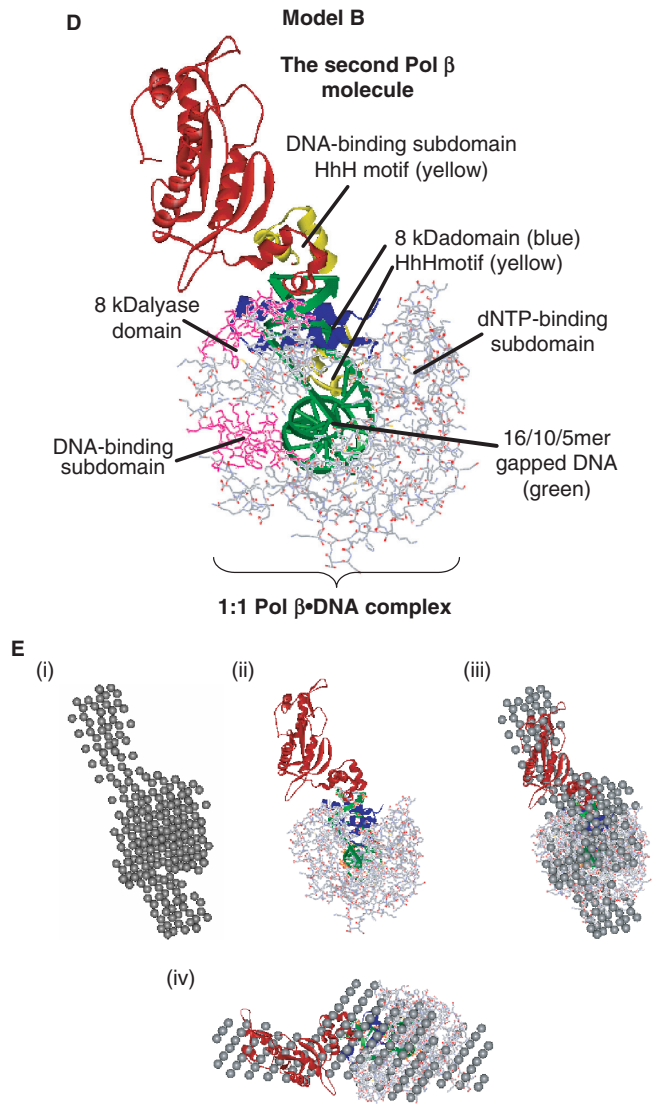

Figure 5. Continued.

Functional relevance. In model B, the 8 kDa domain of the second Pol β molecule binds the downstream duplex DNA and the nascent base pair binding pocket of the 1 : 1 Pol β–DNA complex (Figure 5D). However, in model A, the dNTP-binding and catalytic subdomains of the second Pol β molecule bind the upstream duplex DNA and are away from the binding pocket (Figure 5C). Considering the proposed function of the second Pol β molecule in the 5′-dRP lyase reaction as addressed in Discussion, model B is more functionally relevant.

Pol β-DNA interactions. Two HhH motifs are identified in Pol β; residues 55–79 in the 8 kDa lyase domain and 92–118 in the DNA-binding subdomain (shown in magenta in Figure 5D) (33). The HhH motifs have been identified in many proteins that bind either single- or double-strand DNA in a sequence nonspecific behavior (36). Considering the location of the DNA-binding motif, model B shown in Figure 5D likely represents the structure of the 2 : 1 complex, where the 8 kDa lyase domain of the second Pol β molecule (the HhH motif of the second Pol β molecule is shown in yellow) interacts with the downstream double strand of DNA and also most likely with the Pol β molecule in the 1 : 1 complex. In contrast, no DNA-binding motif can be identified in the dNTP-binding or/and the DNA-binding subdomain as shown in the structural model A. Thus, DNA binding is likely to be non-specific in model A.

To verify the conclusions drawn above, we compared the modeled structures built by DAMMIN (Figure 5B) and SASREF (Figure 5C and D). We have built the DAMMIN models of the 1 : 1 complex and the DAMMIN and GASBOR model of the free Pol β, and the reconstructed models closely resemble the crystal structures (data not shown). As shown in Figure 5E, the low-resolution DAMMIN model of the 2 : 1 complex can be well superimposed onto the high-resolution SASREF model. Furthermore, the predicted scattering pattern of the SASREF model fits the experimentally determined SAXS data well (Figure S6).

Based on our high-resolution reconstructed model of the 2 : 1 complex, it is predicted that DNA binds both Pol β molecules through the HhH motifs, though the DNA-induced conformational change is evident only for the Pol β molecule in the 1 : 1 complex. As described earlier in Results section, when using the 'two-body' modeling (with fixed conformation of the full-length Pol β and the 1 : 1 complex), SASREF can rarely generate the model B-like modeled structure (at most once every twenty runs), where the 8 kDa domain binds in the vicinity of the nascent base pair binding pocket of the 1 : 1 complex, and the fit is rather poor compared to the 'three-body' modeling. The results imply that either some (small) degree of the conformational change may occur in the second Pol β molecule when it binds DNA with the HhH motif in the 8 kDa domain, or the 8 kDa is very flexible and the crystal structure of free Pol β only represents one of the conformations in solution. The former scenario is consistent with binding of Pol β to the 5′-phosphate group of the downstream oligonucleotide contributing to the 8 kDa domain closure (7). The latter is supported by our SAXS data because the calculated SAXS curve derived from the crystal structure does not readily fit the experimental data in the Q-range $>0.12\,\text{Å}^{-1}$ (data not shown), suggesting that the deviation may be due to a floppy link between the lyase and polymerase domains. More studies are required for further clarification of this issue.

DISCUSSION

Advancement from previous reports of 2 : 1 Pol β–DNA complexes

The advancements of our reported 2 : 1 complex studies are summarized as follows. First, even though 2 : 1 and higher order Pol β–DNA complexes have been reported previously (3,4,37–40), this work is the first to provide structural information, and to show that the two Pol β molecules bind to the same site of DNA, and that the two enzyme molecules have different conformations in

the complex. Second, our structural model (Figure 5D) indicates that the second Pol β molecule contacts the nascent base pair binding pocket of the 1 : 1 Pol β–DNA complex with the 8 kDa domain (discussed below). This is the first time the structural detail for a 2 : 1 complex is provided. The different DNA-binding surface revealed in our model can explain different binding affinities of the two Pol β molecules in the 2 : 1 complex, and also correlate with the ionic strength sensitivity of the second Pol β molecule binding to the 1 : 1 complex. Third, it is important to note that not all 2 : 1 complexes are the same. The 2 : 1 (and higher order) complexes observed for Pol β with longer DNA (4) may involve two or more enzyme molecules binding at different sites of DNA. We have performed SV studies with a longer 1 nt gapped DNA, 45-mer template/25-mer primer/19-mer downstream primer (45/25/19-mer), and found that more than two Pol β molecules bind to DNA in the lower salt (~0.1 M KCl) buffer, but only 1 : 1 complex is observed in high ionic strength (~0.4 M KCl) (data not shown). Likewise, a larger Pol X–DNA complex was also observed with longer DNA in our lab (Kumar,S., unpublished data) and others (41). The structures of the higher order Pol β–DNA or ASFV Pol X–DNA complexes with longer DNA remain to be characterized.

Structural comparisons of the ASFV Pol X–DNA complex with the Pol β–DNA complexes

Our results show that a distinct strategy is employed by ASFV Pol X to interact with DNA compared to Pol β and many other DNA polymerases. While Pol β–DNA interactions involve mainly hydrogen bonds between the protein helices in the HhH motifs and the sugar phosphate backbone of DNA, ASFV Pol X binds DNA using the electrostatic interactions through two positively charged regions: the αC helix in the catalytic subdomain interacts with the downstream primer strand/downstream duplex DNA, and the αE helix in the dNTP-binding subdomain binds to the primer strand/upstream duplex DNA (Figure 2D). Our data also confirm the proposed ASFV Pol X–DNA-binding interface suggested by the chemical shift perturbation in the 2D-[^{1}H,^{15}N]-HSQC NMR studies by Tsai and coworkers (9). Furthermore, the positively charged regions in the αC helix of the catalytic subdomain and the αE helix of the dNTP-binding subdomain are presumably the two ssDNA-binding sites detected in the recent fluorescence binding studies of ASFV Pol X–DNA interactions by Jezewska *et al.* (41,42), who reported that the predicted single-strand DNA-binding sites are located asymmetrically within the ASFV Pol X molecule.

The 2 : 1 Pol β–DNA complex is likely the more active form for previous *in vitro* kinetic studies

In this report, we showed that the 2 : 1 Pol β–DNA complex is the predominant form in the presence of excess Pol β relative to DNA, while the 1 : 1 Pol β–DNA complex is the only existing form when DNA is in excess or when the ionic strength is high (>0.4 M KCl). A review of literature indicates that Pol β should exist in the 2 : 1 form predominantly under the conditions used for many pre-steady-state kinetic studies, for example, 1 or 10 mM DTT, 0.1 M KCl, with or without 10% glycerol, 50 mM MOPS buffer at pH 7.0 used in Bakhtina *et al.* (43) and in this study. Furthermore, there have been documentations in the literature that the nucleotidyl transferase activity of Pol β is enhanced when the enzyme is in excess of DNA: (i) pre-steady-state studies (15) showed that when [Pol β] is ~1/2 [DNA], corresponding to the 1 : 1 complex formation described in this report, the active form of the Pol β–DNA complex seems to be close to half of the enzyme concentration; (ii) in the report by Dunlap *et al.* (44), a [Pol β]/[DNA] ratio of 2 : 1 was chosen to form the Pol β–DNA complex because excess amount of enzyme was required to fully saturate the DNA substrate; and (iii) pre-steady-state studies of I260Q variant of Pol β (45) showed that the product formed in the burst phase by I260Q is ~50–60% of the enzyme concentration.

5′-dRP lyase activity of Pol β is enhanced in conditions favoring the 2 : 1 complex

Base excision repair (BER) is proposed to be a sequential process (46), in which the nucleotidyl transferase activity of Pol β catalyzes single nucleotide gap-filling synthesis, while the 5′-dRP lyase activity of Pol β removes the 5′-terminal abasic deoxyribose phosphate (5′-dRP) moiety of the downstream strand. The nucleotidyl transferase reaction can occur before or after the 5′-dRP lyase reaction takes place (7). Our structural model of the 2 : 1 complex in Figure 6A implies that by formation of the 2 : 1 complex, the damaged DNA substrate can be efficiently repaired by passing the resulting DNA product through one active site to the next. We hypothesize that the second Pol β molecule functions as the 5′-dRP lyase and the first Pol β molecule in the 1 : 1 complex is the nucleotidyl transferase. Several previous reports are consistent with our proposed mechanism: (i) it has been reported (47–49) that the isolated 8 kDa domain, not the truncated 31 kDa polymerase domain, can function as a 5′-dRP lyase, supporting the second Pol β molecule processing the lyase reaction; (ii) approximately 5-fold increase in the 5′-dRP lyase activity was reported when Pol β is in excess relative to DNA (47,48,50); (iii) the 5′-dRP lyase activity of Pol β (48) is Mg^{2+}-independent. Our studies showed that binding of the second Pol β molecule is tighter when Mg^{2+} was omitted and (iv) most importantly, in the crystal structures of the ternary complexes of Pol β (7,8) (binding of MgdNTP to the 1 : 1 Pol β–DNA complex), the 8 kDa domain is not at the optimal position and 5′-dRP group is far away from the Schiff base nucleophile (Lys^{72}), suggesting that the Pol β molecule that catalyzes the nucleotidyl transfer may not be the same one that catalyzes the 5′-dRP lyase reaction.

ASFV may use a separate 5′-dRP lyase instead of a 2 : 1 Pol X–DNA complex

In contrast to Pol β, ASFV Pol X can only form a 1 : 1 complex with DNA. It also showed no detectable 5′-dRP lyase activity as reported by Garcia-Escudero *et al.* (51). The authors proposed that either 5′-dRP lyase is not required or a different enzyme functions as a 5′-dRP lyase for short-patch BER in ASFV if the same short-patch

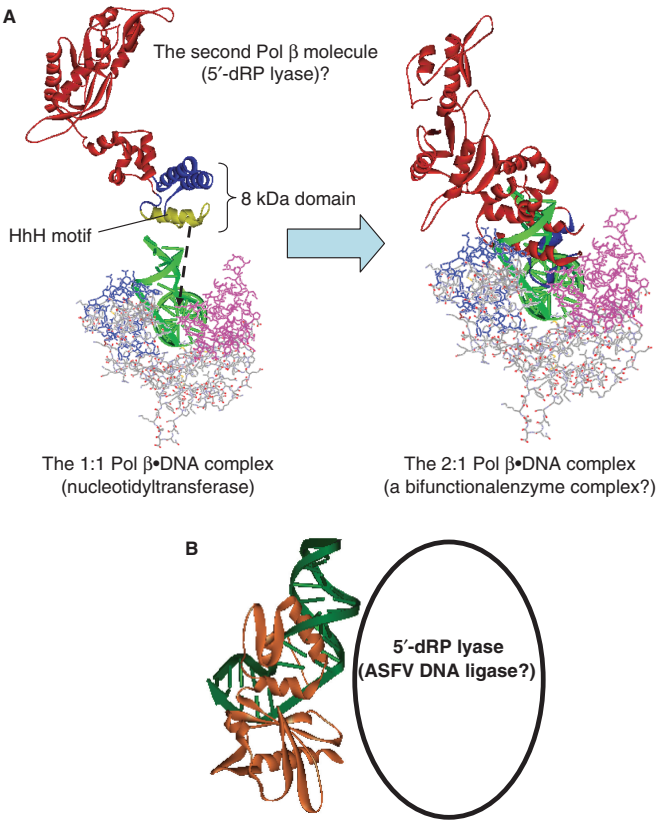

Figure 6. Proposed biological roles of the 2:1 Pol β–DNA complex and 1:1 ASFV Pol X–DNA complex in the BER pathway. (**A**) The HhH motifs in the 1:1 Pol β–DNA complex (lower left), the 8 kDa lyase domain of the second Pol β molecule (upper left), and the 2:1 Pol β–DNA complex (right) are highlighted in blue, and the fingers subdomain is labeled in pink. We propose that the first Pol β in the 2:1 complex functions as a nucleotidyl transferase, and the second Pol β molecule works as a 5′-deoxyribose phosphodiesterase interacting with the DNA damaged site. (**B**) Proposed interactions of a viral 5′-deoxyribose phosphodiesterase interacting with the ASFV Pol X–DNA complex in the viral BER pathway.

BER is followed by ASFV as in mammalian cells. If the latter pathway is operational in viral BER, the preliminary studies in our laboratory suggested that the 5′-dRP lyase activity is likely performed by the ASFV DNA ligase (11). It is consistent with the previous studies (52,53) of borohydride trapping and 5′-dRP release assays showing that several DNA ligases can function as a lyase and remove the 5′-dRP moiety. As shown in our structural model (Figure 2B), most of the DNA moiety is not enclosed in the ASFV Pol X–DNA complex, and a rather open binding interface is accessible for other protein(s) to interact with DNA and ASFV Pol X. Thus, one can postulate that ASFV DNA ligase interacts with the ASFV Pol X–DNA complex, removes the 5′-dRP moiety, and ligates the nicked DNA substrate to complete the BER for this virus (Figure 6B).

The 2 : 1 enzyme–DNA complexes reported in other DNA polymerases

A survey of the literature suggests that the 2 : 1 enzyme–DNA complexes could also be functionally relevant in other DNA polymerases: (i) the report of the 2 : 1 KF–DNA complex (5) proposed that the first KF molecule is responsible for nucleotidyl transferase (5′–3′ polymerase) activity and the second KF molecule possibly functions as an editing (exonuclease) enzyme. Thus even though DNA polymerase I and Pol β have different biological roles, they may both employ the 2 : 1 complex to perform multiple functions. Our studies provide the first structural information for such complexes. (ii) Like Pol β, more than 2-fold excess amount of enzyme over DNA was used in the stopped-flow fluorescence studies of KF (54). (iii) Only approximately 40–50% of DNA substrate was converted into product in the active site titration studies of HIV-1 reverse transcriptase (55) and T7 DNA polymerase (56). (iv) Two other DNA polymerases, human Pol λ (57) and Pol ι (58), also exhibited the Mg^{2+}-independent 5′-dRP lyase activity, and analogous to Pol β, higher catalytic activity was reported in the excess of enzyme relative to DNA. These two DNA polymerases were proposed to be involved in DNA repair (59) because they display 5′-dRP lyase activity, and it remains to be investigated if a 2 : 1 complex is formed in these enzymes.

CONCLUSION

In this report, we have performed systematic studies on the DNA polymerase–DNA complexes under different reaction conditions, and characterized the structure of the 2 : 1 Pol β–DNA complex and 1 : 1 ASFV Pol X–DNA complex with the gapped DNA under the conditions used for functional studies. This solution structural information is otherwise un-obtainable, and provides valuable insight into the *in vivo* functions of both enzymes in the BER pathway. When applied to other DNA repair complexes, the potential significance will be enormous.

SUPPLEMENTARY DATA

Supplementary Data are available at NAR Online.

ACKNOWLEDGEMENTS

We thank Dr Liang Guo (APS) for SAXS beamline support and data collection at BioCAT 18-ID; Dr Mei-I Su (OSU) for NMR studies and useful suggestions on ASFV Pol X studies; Dr Chunhua Yuan (OSU) and Dr Wen-Jin Wu (AS) for NMR studies; and Mr Sandeep Kumar for assisting the preparations of ASFV Pol X samples. This work was supported by the National Science Council Grant 95-2745-B and the National Institutes of Health Grants GM43268 and CA69472 (to M.-D.T.). K.-H.T. was partially supported by the Distinguished Academia Sinica Postdoctoral Fellowship. SAXS experiments were carried out at BL 4-2 of the Stanford Synchrotron Radiation Laboratory (SSRL) and at BioCAT 18-ID of the Advanced Photon Sources (APS), supported by the National Institutes of Health and the Department of Energy. NMR experiments were performed at the NMR facility of the Ohio State University and at the High-Field Biomacromolecular

NMR Core Facility supported by the National Research Program for Genomic Medicine of Taiwan. Funding to pay the Open Access publication charges for this article was provided by Genomics Research Center.

Conflict of interest statement. None declared.

REFERENCES

1. Sawaya,M.R., Pelletier,H., Kumar,A., Wilson,S.H. and Kraut,J. (1994) Crystal structure of rat DNA polymerase beta: evidence for a common polymerase mechanism. *Science*, **264**, 1930–1935.
2. Steitz,T.A., Smerdon,S.J., Jager,J. and Joyce,C.M. (1994) A unified polymerase mechanism for nonhomologous DNA and RNA polymerases. *Science*, **266**, 2022–2025.
3. Tsoi,P.Y. and Yang,M. (2002) Kinetic study of various binding modes between human DNA polymerase beta and different DNA substrates by surface-plasmon-resonance biosensor. *Biochem. J.*, **361**, 317–325.
4. Rajendran,S., Jezewska,M.J. and Bujalowski,W. (2001) Recognition of template-primer and gapped DNA substrates by the human DNA polymerase beta. *J. Mol. Biol.*, **308**, 477–500.
5. Bailey,M.F., Van der Schans,E.J. and Millar,D.P. (2007) Dimerization of the Klenow fragment of Escherichia coli DNA polymerase I is linked to its mode of DNA binding. *Biochemistry*, **46**, 8085–8099.
6. Bujalowski,W. (2006) Thermodynamic and kinetic methods of analyses of protein-nucleic acid interactions. From simpler to more complex systems. *Chem. Rev.*, **106**, 556–606.
7. Beard,W.A. and Wilson,S.H. (2006) Structure and mechanism of DNA polymerase Beta. *Chem. Rev.*, **106**, 361–382.
8. Sawaya,M.R., Prasad,R., Wilson,S.H., Kraut,J. and Pelletier,H. (1997) Crystal structures of human DNA polymerase beta complexed with gapped and nicked DNA: evidence for an induced fit mechanism. *Biochemistry*, **36**, 11205–11215.
9. Showalter,A.K., Byeon,I.J., Su,M.I. and Tsai,M.D. (2001) Solution structure of a viral DNA polymerase X and evidence for a mutagenic function. *Nat. Struct. Biol.*, **8**, 942–946.
10. Maciejewski,M.W., Shin,R., Pan,B., Marintchev,A., Denninger,A., Mullen,M.A., Chen,K., Gryk,M.R. and Mullen,G.P. (2001) Solution structure of a viral DNA repair polymerase. *Nat. Struct. Biol.*, **8**, 936–941.
11. Showalter,A.K., Lamarche,B.J., Bakhtina,M., Su,M.I., Tang,K.H. and Tsai,M.D. (2006) Mechanistic comparison of high-fidelity and error-prone DNA polymerases and ligases involved in DNA repair. *Chem. Rev.*, **106**, 340–360.
12. Beard,W.A. and Wilson,S.H. (2001) DNA polymerases lose their grip. *Nat. Struct. Biol.*, **8**, 915–917.
13. Showalter,A.K. and Tsai,M.D. (2001) A DNA polymerase with specificity for five base pairs. *J. Am. Chem. Soc.*, **123**, 1776–1777.
14. Kraynov,V.S., Showalter,A.K., Liu,J., Zhong,X. and Tsai,M.D. (2000) DNA polymerase beta: contributions of template-positioning and dNTP triphosphate-binding residues to catalysis and fidelity. *Biochemistry*, **39**, 16008–16015.
15. Werneburg,B.G., Ahn,J., Zhong,X., Hondal,R.J., Kraynov,V.S. and Tsai,M.D. (1996) DNA polymerase beta: pre-steady-state kinetic analysis and roles of arginine-283 in catalysis and fidelity. *Biochemistry*, **35**, 7041–7050.
16. Smolsky,I.L., Liu,P., Niebuhr,M., Ito,K., Weiss,T.M. and Tsuruta,H. (2007) Biological small-angle x-ray scattering facility at the Stanford synchrotron radiation laboratory. *J. Appl. Crystallogr.*, **40**, S453–S458.
17. Fischetti,R., Stepanov,S., Rosenbaum,G., Barrea,R., Black,E., Gore,D., Heurich,R., Kondrashkina,E., Kropf,A.J. *et al.* (2004) The BioCAT undulator beamline 18ID: a facility for biological non-crystalline diffraction and X-ray absorption spectroscopy at the Advanced Photon Source. *J. Synchrotron. Radiat.*, **11**, 399–405.
18. Tang,K.H., Guo,H., Yi,W., Tsai,M.D. and Wang,P. (2007) Investigation of the conformational states of Wzz and the Wzz•O-antigen complex under near-physiological conditions. *Biochemistry*, **46**, 11744–11752.
19. Konarev,P.V., Volkov,V.V., Sokolova,A.V., Koch,M.H.J. and Svergun,D.I. (2003) PRIMUS: a windows PC-based system for small-angle scattering data analysis. *J. Appl. Cryst.*, **36**, 1277–1282.
20. Koch,M.H., Vachette,P. and Svergun,D.I. (2003) Small-angle scattering: a view on the properties, structures and structural changes of biological macromolecules in solution. *Q. Rev. Biophys.*, **36**, 147–227.
21. Svergun,D.I. (1992) Determination of the regularization parameter in indirect-transform methods using perceptual criteria. *J. Appl. Cryst.*, **25**, 495–503.
22. Guinier,A. and Fournet,G. (1955) *Small-Angle Scattering of X-Rays*. John Wiley & Sons, Inc., New York.
23. Svergun,D.I. (1999) Restoring low resolution structure of biological macromolecules from solution scattering using simulated annealing. *Biophys. J.*, **76**, 2879–2886.
24. Svergun,D.I., Petoukhov,M.V. and Koch,M.H. (2001) Determination of domain structure of proteins from X-ray solution scattering. *Biophys. J.*, **80**, 2946–2953.
25. Petoukhov,M.V. and Svergun,D.I. (2005) Global rigid body modeling of macromolecular complexes against small-angle scattering data. *Biophys. J.*, **89**, 1237–1250.
26. Maciejewski,M.W., Liu,D., Prasad,R., Wilson,S.H. and Mullen,G.P. (2000) Backbone dynamics and refined solution structure of the N-terminal domain of DNA polymerase beta. Correlation with DNA binding and dRP lyase activity. *J. Mol. Biol.*, **296**, 229–253.
27. Pelletier,H. and Sawaya,M.R. (1996) Characterization of the metal ion binding helix-hairpin-helix motifs in human DNA polymerase beta by X-ray structural analysis. *Biochemistry*, **35**, 12778–12787.
28. Kozin,M.B. and Svergun,D.I. (2001) Automated matching of high- and low-resolution structural modles. *J. Appl. Crystallogr.*, **34**, 33–41.
29. Svergun,D.I., Barberato,C. and Koch,M.H.J. (1995) CRYSOL - a program to Evaluate X-ray Solution Scattering of Biological Macromolecules from Atomic Coordinates. *J. Appl. Cryst.*, **28**, 768–773.
30. Schuck,P. (2000) Size-distribution analysis of macromolecules by sedimentation velocity ultracentrifugation and lamm equation modeling. *Biophys. J.*, **78**, 1606–1619.
31. Schuck,P. (2003) On the analysis of protein self-association by sedimentation velocity analytical ultracentrifugation. *Anal. Biochem.*, **320**, 104–124.
32. Garcia De La Torre,J., Huertas,M.L. and Carrasco,B. (2000) Calculation of hydrodynamic properties of globular proteins from their atomic-level structure. *Biophys. J.*, **78**, 719–730.
33. Pelletier,H., Sawaya,M.R., Wolfle,W., Wilson,S.H. and Kraut,J. (1996) Crystal structures of human DNA polymerase beta complexed with DNA: implications for catalytic mechanism, processivity, and fidelity. *Biochemistry*, **35**, 12742–12761.
34. Ahn,J., Kraynov,V.S., Zhong,X., Werneburg,B.G. and Tsai,M.D. (1998) DNA polymerase beta: effects of gapped DNA substrates on dNTP specificity, fidelity, processivity and conformational changes. *Biochem. J.*, **331**, 79–87.
35. Beard,W.A., Prasad,R. and Wilson,S.H. (2006) Activities and mechanism of DNA polymerase beta. *Methods Enzymol.*, **408**, 91–107.
36. Doherty,A.J., Serpell,L.C. and Ponting,C.P. (1996) The helix-hairpin-helix DNA-binding motif: a structural basis for non-sequence-specific recognition of DNA. *Nucleic Acids Res.*, **24**, 2488–2497.
37. Rajendran,S., Jezewska,M.J. and Bujalowski,W. (2001) Multiple-step kinetic mechanisms of the ssDNA recognition process by human polymerase beta in its different ssDNA binding modes. *Biochemistry*, **40**, 11794–11810.
38. Jezewska,M.J., Rajendran,S., Galletto,R. and Bujalowski,W. (2001) Kinetic mechanisms of rat polymerase beta-ssDNA interactions. Quantitative fluorescence stopped-flow analysis of the formation of the (Pol beta)(16) and (Pol beta)(5) ssDNA binding mode. *J. Mol. Biol.*, **313**, 977–1002.
39. Jezewska,M.J., Rajendran,S. and Bujalowski,W. (2001) Energetics and specificity of Rat DNA polymerase beta interactions with template-primer and gapped DNA substrates. *J. Biol. Chem.*, **276**, 16123–16136.

40. Rajendran,S., Jezewska,M.J. and Bujalowski,W. (1998) Human DNA polymerase beta recognizes single-stranded DNA using two different binding modes. *J. Biol. Chem.*, **273**, 31021–31031.
41. Jezewska,M.J., Bujalowski,P.J. and Bujalowski,W. (2007) Interactions of the DNA polymerase X from African swine fever virus with gapped DNA substrates. Quantitative analysis of functional structures of the formed complexes. *Biochemistry*, **46**, 12909–12924.
42. Jezewska,M.J., Marcinowicz,A., Lucius,A.L. and Bujalowski,W. (2006) DNA polymerase X from African swine fever virus: quantitative analysis of the enzyme-ssDNA interactions and the functional structure of the complex. *J. Mol. Biol.*, **356**, 121–141.
43. Bakhtina,M., Lee,S., Wang,Y., Dunlap,C., Lamarche,B. and Tsai,M.D. (2005) Use of viscogens, dNTPalphaS, and rhodium(III) as probes in stopped-flow experiments to obtain new evidence for the mechanism of catalysis by DNA polymerase beta. *Biochemistry*, **44**, 5177–5187.
44. Dunlap,C.A. and Tsai,M.D. (2002) Use of 2-aminopurine and tryptophan fluorescence as probes in kinetic analyses of DNA polymerase beta. *Biochemistry*, **41**, 11226–11235.
45. Starcevic,D., Dalal,S., Jaeger,J. and Sweasy,J.B. (2005) The hydrophobic hinge region of rat DNA polymerase beta is critical for substrate binding pocket geometry. *J. Biol. Chem.*, **280**, 28388–28393.
46. Wilson,S.H. and Kunkel,T.A. (2000) Passing the baton in base excision repair. *Nat. Struct. Biol.*, **7**, 176–178.
47. Prasad,R., Beard,W.A., Chyan,J.Y., Maciejewski,M.W., Mullen,G.P. and Wilson,S.H. (1998) Functional analysis of the amino-terminal 8-kDa domain of DNA polymerase beta as revealed by site-directed mutagenesis. DNA binding and 5′-deoxyribose phosphate lyase activities. *J. Biol. Chem.*, **273**, 11121–11126.
48. Prasad,R., Beard,W.A., Strauss,P.R. and Wilson,S.H. (1998) Human DNA polymerase beta deoxyribose phosphate lyase. Substrate specificity and catalytic mechanism. *J. Biol. Chem.*, **273**, 15263–15270.
49. Matsumoto,Y., Kim,K., Katz,D.S. and Feng,J.A. (1998) Catalytic center of DNA polymerase beta for excision of deoxyribose phosphate groups. *Biochemistry*, **37**, 6456–6464.
50. Prasad,R., Batra,V.K., Yang,X.P., Krahn,J.M., Pedersen,L.C., Beard,W.A. and Wilson,S.H. (2005) Structural insight into the DNA polymerase beta deoxyribose phosphate lyase mechanism. *DNA Repair*, **4**, 1347–1357.
51. Garcia-Escudero,R., Garcia-Diaz,M., Salas,M.L., Blanco,L. and Salas,J. (2003) DNA polymerase X of African swine fever virus: insertion fidelity on gapped DNA substrates and AP lyase activity support a role in base excision repair of viral DNA. *J. Mol. Biol.*, **326**, 1403–1412.
52. Pinz,K.G. and Bogenhagen,D.F. (1998) Efficient repair of abasic sites in DNA by mitochondrial enzymes. *Mol. Cell. Biol.*, **18**, 1257–1265.
53. Bogenhagen,D.F. and Pinz,K.G. (1998) The action of DNA ligase at abasic sites in DNA. *J. Biol. Chem.*, **273**, 7888–7893.
54. Purohit,V., Grindley,N.D. and Joyce,C.M. (2003) Use of 2-aminopurine fluorescence to examine conformational changes during nucleotide incorporation by DNA polymerase I (Klenow fragment). *Biochemistry*, **42**, 10200–10211.
55. Suo,Z., Lippard,S.J. and Johnson,K.A. (1999) Single d(GpG)/cis-diammineplatinum(II) adduct-induced inhibition of DNA polymerization. *Biochemistry*, **38**, 715–726.
56. Tsai,Y.C. and Johnson,K.A. (2006) A new paradigm for DNA polymerase specificity. *Biochemistry*, **45**, 9675–9687.
57. Garcia-Diaz,M., Bebenek,K., Kunkel,T.A. and Blanco,L. (2001) Identification of an intrinsic 5′-deoxyribose-5-phosphate lyase activity in human DNA polymerase lambda: a possible role in base excision repair. *J. Biol. Chem.*, **276**, 34659–34663.
58. Bebenek,K., Tissier,A., Frank,E.G., McDonald,J.P., Prasad,R., Wilson,S.H., Woodgate,R. and Kunkel,T.A. (2001) 5′-Deoxyribose phosphate lyase activity of human DNA polymerase iota in vitro. *Science*, **291**, 2156–2159.
59. Bebenek,K. and Kunkel,T.A. (2004) Functions of DNA polymerases. *Adv. Protein Chem.*, **69**, 137–165.